RSC Advances

PAPER

Cite this: *RSC Adv.*, 2023, **13**, 22789

Langmuir monolayer of lysozyme at variable subphase pH conditions: a comprehensive study on structure, morphology and hysteresis behaviour

Himadri Nath,[ab] Raktim J. Sarmah[a] and Sarathi Kundu *[ab]

Formation of a pure Langmuir monolayer of lysozyme at the air–water interface and its investigation by means of a surface pressure (π)–mean molecular area (A) isotherm has been accomplished under different subphase pH conditions. A normalized area–time curve confirms the stable nature of the lysozyme monolayer whose compressibility variation with an increased surface pressure at specific subphase pH has also been studied from π–A isotherms. The monolayers exhibit irreversible hysteresis behaviour irrespective of subphase pH conditions, as evidenced from successive compression–expansion π–A isotherm cycles. Comparison of surface thermodynamics under hysteresis with subphase pH variation confirms that the monolayer at subphase pH $\approx$ 4.0 involves a greater amount of energy to attain and retain the ordered and compact monolayer than the other two pH conditions (pH $\approx$ 7.0 and 9.5). *In situ* visualization of lysozyme monolayers by Brewster angle microscopy suggests the homogeneous and stripe-like pattern formation at lower and higher surface pressure respectively. Further investigations of lysozyme films at solid surfaces have been carried out with atomic force microscopy and X-ray reflectivity (XRR) analysis. Structural reversibility of lysozyme molecules under compression–expansion–compression of the monolayer is revealed from the comparison of height profiles of AFM images and electron density profiles as extracted from XRR analysis of the films deposited during both first and second compressions of the monolayer. The mechanism of the structural rearrangement of lysozyme molecules with surface pressure variation at different subphase pH is explored, correlating macroscopic and microscopic information.

Received 3rd June 2023
Accepted 15th July 2023

DOI: 10.1039/d3ra03710j

rsc.li/rsc-advances

1. Introduction

Proteins are the fundamental biomolecules that play a pivotal role in the survival of all living organisms. They transform into functionally active unique 3D complex molecules through subsequent levels of folding of the precise amino acids sequences.[1–3] The functional activity of these macromolecules is primarily dependent on their structure, which can be controlled through the variation of physiochemical parameters such as temperature, pH, ionic strength, solvent polarity, presence of additives, *etc.*[4–7] The surface charge of the proteins can be adjusted by varying the pH of the protein solution as it changes the microenvironment of proteins. Charged functional groups on the protein surface are organized in 'patches' rather than being evenly distributed, creating a complicated mosaic. At a particular value of pH commonly defined as the isoelectric point (pI), protein has a neutral charge value, however, below and above this pI value it carries positive and negative surface charges respectively.[8] Further, the presence of polar, non-polar, and ionic regions of proteins leads to their adsorption on various surfaces from bio-membranes to solid substrates. The mechanism of adsorption of these protein molecules to various surfaces and also its crystallization depends upon the structure, conformation, function, *etc.*[9,10] In-depth investigations on such properties and their alteration under varying physicochemical environments help to understand many existing health issues such as Alzheimer's and Parkinson's diseases.[11,12]

In the recent past, the exploration on proteins has drawn tremendous interest among various research disciplines due to their wide variety of applications ranging from the food industry to device manufacturing. For instance, proteins are widely used as an emulsifier in food processing or as an edible coating to cut out moisture in food products.[13] In addition to this, proteins also have immense applications in different areas such as tissue engineering, pharmaceuticals, drug delivery, manufacturing of devices like biosensors, bio-photonic devices for medical applications, *etc.*[14,15] Amongst different proteins, globular proteins are composed of a hydrophobic core surrounded by polar or ionic amino acid groups which makes them highly soluble in water. Lysozyme is one such globular protein which is also regarded as a model for exploring the structures and

[a]*Soft Nano Laboratory (SNL), Physical Sciences Division, Institute of Advanced Study in Science and Technology (IASST), Vigyan Path, Paschim Boragaon, Garchuk, Guwahati, Assam 781035, India. E-mail: sarathi.kundu@gmail.com*

[b]*Academy of Scientific and Innovative Research (AcSIR), Ghaziabad 201002, India*

functions of the protein. As its pI is approximately 11.0, it behaves as a positively charged molecule under physiological conditions.[16] The primary structure of lysozyme comprises 129 amino acid residues with 14.3 kDa molecular mass.[17] The presence of four disulfide bonds makes the 3D structure of this protein unusually compact and highly stable.[18,19] This globular protein is abundantly found in egg white (about 3.4% of total protein) and almost all secretions in mammals like tears, saliva, and milk. Egg white lysozyme is the most widely studied protein as its structure is only differing by 40% from human lysozyme.[20,21] It is due to its antimicrobial property for which it is extensively used in the fields of food technology, cosmetics, pharmaceuticals, *etc.*[13,22,23]

Despite of the water solubility of the globular proteins, relatively bigger size globular proteins can also form dense monolayers at the air–water interface.[24] It is possible to assemble protein molecules at the air–water interface as monolayer either by injecting protein molecules into the aqueous subphase followed by adsorption to the interface called Gibbs monolayer or by spreading protein molecules on the water surface called Langmuir monolayer.[25–28] Such monolayers at the air–water interface can be investigated further after transferring onto some solid surfaces by the method called Langmuir–Blodgett (LB) method of film deposition. Although different immobilization methods such as drop-casting, spin-coating, dip-coating, LB methods, *etc.* have been used,[29,30] however, among them LB method serves as a promising technique that allows ordered deposition of films with closely-packed structures and tunable film thickness at the molecular level.[27,31] Furthermore, protein films fabricated through this technique have significantly better mechanical and thermal stability.[32,33] In case of smaller globular proteins like lysozyme, monolayer film can be formed at the air–water interface under different adsorption conditions as a consequence of various interactions including electrostatic, hydrophobic, van der Waals, intermolecular bonds, *etc.* Studies on lysozyme layer adsorbed at an air–water interface using neutron-reflection measurements suggest that lysozyme retains its globular structure at interface independent of its bulk concentration.[34–36] In contrast, the FTIR study reveals the conformation variation of lysozyme molecules with high antiparallel β content upon adsorption at the air–water interface.[37] Elastic properties of the lysozyme layer adsorbed at the air–water interface covered with the surfactant ETHT 4001 was also investigated.[38] Literature review advocates that a considerable amount of research work was reported on the study of lysozyme film at the air–water interface which deals with the adsorption process. However, very few works have been published on the Langmuir monolayer of lysozyme films where molecules are spread on the water surface from a specific solution. Yamashita *et al.* stated that lysozyme cannot form a stable monolayer spread over the aqueous subphase.[39] On the contrary, Thakur *et al.* reported the formation of a Langmuir monolayer of lysozyme at elevated subphase pH and in the presence of 3 mM salt (KCl) concentration.[40] Potassium iodide (KI) has also been used as a precipitant by another group in fabricating a multilayer film of lysozyme.[41] Pechkova *et al.* reported that lysozyme films fabricated from its Langmuir monolayer can be considered as a nano template for the growth of different protein crystals.[42] In addition, it is also evidenced that lysozyme retains its structural stability up to a temperature of around 200 °C when immobilized as an LB film.[33] So far the formation of Langmuir monolayer of lysozyme is possible only if concentrated aqueous solution is used for spreading the molecules instead of dilute solution. Although the Langmuir monolayer of lysozyme from the concentrated solution or in the presence of salt is studied, still formation of pure lysozyme Langmuir monolayer at air–water interface from dilute solvent solution has not been reported yet and needs further exploration in this regard for a better understanding. The purpose of our current study is to provide key information on structures and morphologies of pure lysozyme Langmuir monolayers on the aqueous surface under different pH conditions and its related surface thermodynamics under compression–expansion surface pressure (π)–mean molecular area (A) isotherms which in turn may be helpful to understand various biological mechanisms like pulmonary compliance, *etc.* and also in potential applications such as bio coating and protein nano template fabrication for protein crystallization.

In the present study, pure lysozyme Langmuir monolayers are formed by spreading on the water surface using the dilute solution of protein mixed in specific solvent ratios. Successive compression–expansion of the protein monolayers is studied by varying certain parameters like surface pressure as well as pH of the sub-phase using the LB method. The compressibility variation of the monolayers under different surface pressure and pH conditions are also studied from the surface pressure (π)–mean molecular area (A) isotherms. The domain patterns formed at the air–water interface are visualized with the help of Brewster angle microscopy (BAM). The protein monolayers formed are deposited on the hydrophilic silicon surface by LB method at different surface pressures and different subphase pH conditions for further characterization. The in-plane morphology and out-of-plane structures of the lysozyme films are characterized by atomic force microscopy (AFM) and X-ray reflectivity (XRR) analysis. Moreover, the stability of the lysozyme monolayer is also explored at pH $\approx$ 7.0 on both aqueous and solid surfaces using BAM, AFM, and XRR analysis. The results obtained from the different experimental methods thus help to explore the mechanism of structural rearrangement of lysozyme molecules with surface pressure and subphase pH variation.

2. Experimental

2.1. Materials

Lysozyme (Sigma-Aldrich, Germany), methanol (Merck, India), chloroform (Sigma-Aldrich, India), ammonium hydroxide (NH_4OH, Merck, 25%), hydrogen peroxide (H_2O_2, 30%, Merck), HCl (35%, Merck, India), and NaOH (Merck, India) were used as received.

2.2. Methods

2.2.1. Preparation of lysozyme solution. 0.5 mg ml^{-1} solution of lysozyme was prepared in a solution mixture containing

40 : 20 : 3 ratio of chloroform, methanol, and water respectively.[43]

2.2.2. Formation of lysozyme monolayer. Using a Hamilton syringe, a specific amount of this lysozyme solution was spread carefully over the aqueous subphase surface in a double-barrier Langmuir trough made of Teflon (dimensions: length × width × height ≈ 56.5 cm × 19.5 cm × 0.5 cm) consisting of a well (dimension: length × width × height ≈ 8.0 cm × 6.0 cm × 5.5 cm) in the middle of the trough. The variation of the surface pressure was monitored using a paper Wilhelmy plate. A time gap of ≈10 min is set before each compression for solvent evaporation and achieving equilibrium condition of the monolayer. For compression and expansion of the monolayer barrier movement was kept constant at 5 mm min^{-1}. All measurements were carried out at room temperature of ≈24 °C. The subphase pH was maintained at ≈4.0, 7.0, and 9.5 by adding the requisite amount of HCl and NaOH solution for different experimental conditions.

2.2.3. Deposition of lysozyme LB films. For deposition, Si (001) substrates are used after making it hydrophilic by boiling in a solution mixture of ammonium hydroxide, hydrogen peroxide, and ultrapure water ($NH_4OH : H_2O_2 : H_2O = 1 : 1 : 2$, by volume) for 7–9 min and then washing with ultrapure water. During the first compression, surface pressure values of 5 mN m^{-1} (lower pressure) and 27 mN m^{-1} (higher pressure) were selected whereas in case of second compression the surface pressure of 5 mN m^{-1} (lower value) was maintained at each subphase pH condition for LB film deposition. Transfer of lysozyme molecules were carried out *via* a single up-stroke of the substrate at a constant dipper speed of 2 mm min^{-1} through the protein monolayer-covered water surface.

2.2.4. Characterization

2.2.4.1. Brewster angle microscopy (BAM). Brewster angle microscopy (BAM, nanofilm EP4) was used for the *in situ* visualization of lysozyme monolayer formed at the water subphase. This instrument is equipped with a solid state laser of 50 mW and a polarizer that emits light of 658 nm wavelength having p-polarized characteristics. A wedge-shaped black colored glass plate was kept at the bottom of the trough to reflect any light transmitted through the subphase out of the optical axis and also to minimize the trough convection. The reflected light is captured using a high-quality, monochrome GigE CCD camera with 1392 × 1040 pixels which is again coupled to a 10× magnification objective, resulting in 2 μm spatial resolution. BAM images of lysozyme films were taken at lower ($\pi \approx 5$ mN m^{-1}), intermediate ($\pi \approx$ 15–20 mN m^{-1}), and higher ($\pi \approx$ 22–26 mN m^{-1}) surface pressure during 1st compression and also at lower surface pressure ($\pi \approx 5$ mN m^{-1}) during 2nd compression as well.

2.2.4.2. Atomic force microscopy (AFM). Surface morphology and roughness of the fabricated films were analyzed through an AFM (AFM, NTEGRA Prima, NT-MDT Technology). Scanning of the films was operated in semi-contact mode with a cantilever made of silicon having ≈11.8 N m^{-1} spring constant.[44] From a single film several portions of 1 μm × 1 μm in area were considered for scanning. The AFM images were processed and analyzed using WSxM software.[45]

2.2.4.3. X-ray reflectivity (XRR) analysis. For XRR measurements of the lysozyme deposited film, X-ray diffractometer (D8 Advanced, Bruker AXS) setup was used. The whole setup consists of a copper (Cu) source along with a Göbel mirror for the selection of enhanced CuK_α radiation (≈1.54 Å) and a NaI scintillation detector for the detection of scattered beam. The data collection was carried out keeping the setup in specular condition by equalizing the reflected angle (θ_r) with the incident angle (θ_i). This condition gives $q_z = 4\pi/\lambda \sin\theta$, where q_z is the vertical component of the wave-vector. Parratt's formalism[46] was employed to analyze the XRR data where it was assumed that each film is a stack of homogeneous layers with the consideration of both surface and interfacial roughness.[47,48] Out-of-plane structures of the deposited films are revealed from electron density profile (EDPs) which is extracted from XRR analysis. This EDPs or electron density variation[47,49] basically signifies in-plane (x–y) average electron density (ρ) as a function of depth (z) and is obtained with high resolution.[47,50,51] For the data fitting, each film was divided into a number of layers including roughness at each interface. The densities of Si substrate and silicon oxide layer formed on its surface were kept constant during data fitting. In all films, three layers model was employed and an instrumental resolution in the form of a Gaussian function and a constant background was also included at the time of data analysis.

3. Results and discussion

The surface pressure-mean molecular area (π–A) isotherms of pure lysozyme monolayer formed at the air–water interface are shown in Fig. 1(a). The isotherms were taken at three different subphase pH values, *i.e.*, at pH ≈ 4.0, 7.0, and 9.5, which are below the pI of lysozyme. Pre-prepared lysozyme solutions when spread over the aqueous subphase results in the formation of stable monolayer film at the air–water interface with the adoption of sideways-on orientation of the lysozyme molecules due to the excess area of the trough.[36] In general, such orientation gives rise to a compact area, A_0, *i.e.*, $\pi \times a \times b \approx 10.30$ nm^2, considering the lysozyme molecule to be a prolate ellipsoid ≈27.8 Å × 11.8 Å × 11.8 Å ($a \times b \times b$).[52] Irrespective of the different pH conditions applied, π–A isotherms of lysozyme monolayers show the lift-off area of ≈13.5 nm^2 per molecule, which is relatively higher in comparison with A_0. The probable reason behind this can be assigned to the electrostatic repulsive interaction amongst lysozyme molecules and the presence of defects or voids in the monolayer. Fig. 1(a) shows that although pH does not have an impact on lift-off area, the rate of increase in surface pressure is such that it results in showing different limiting molecular area with pH variation, which is the extrapolation from the linear part of the π–A isotherm to zero surface pressure. From the isotherms, it is clear that the limiting molecular area increases as the subphase pH approaches towards the isoelectric point, which is in accordance with the outcome as stated by Thakur *et al.*,[40] although the increment is found to be comparatively small in our result. For pH ≈ 4.0, the limiting molecular area is found to be 10.45 nm^2 per molecule, whereas for pH ≈ 7.0 and 9.5 it is nearly 11.4

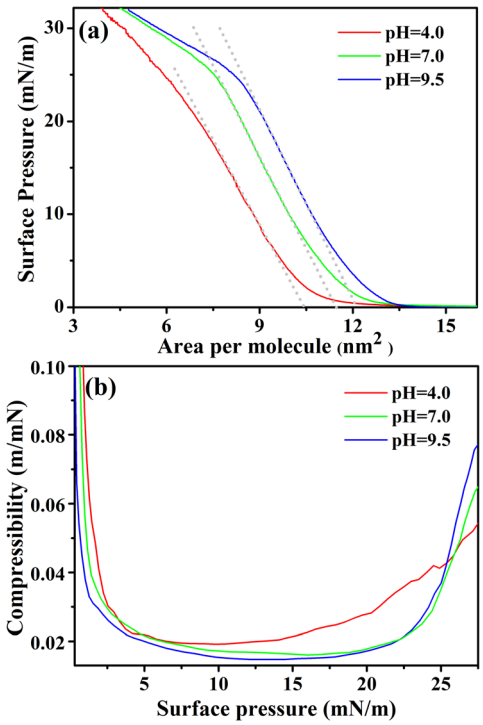

Fig. 1 (a) Surface pressure–mean molecular area (π–A) isotherms of lysozyme monolayer and corresponding; (b) isothermal compressibility (k) as a function of surface pressure (π) at three different subphase pH values, *i.e.* at pH ≈ 4.0 (red color), pH ≈ 7.0 (green color) and pH ≈ 9.5 (blue color).

nm^2 per molecule and 12.2 nm^2 per molecule respectively. Deviation of limiting molecular area from the compact area A_0 may occur for following the specific way of orientation of lysozyme molecules with barrier compression and also for the conformational variation of the lysozyme molecule depending upon the subphase pH conditions. Linear increment of the surface pressure resulted in the formation of plateau-like feature or slope in the isotherms as can be seen from Fig. 1(a), however, the bending nature and the relative pressure associated with the bending is found to vary with the pH conditions. For subphase pH ≈ 4.0, the slope of π–A isotherm starts to change from below $\pi = 20$ mN m^{-1}, while for pH ≈ 7.0 and 9.5 changes in slope start above $\pi = 20$ mN m^{-1}. The degree of bending of the slope or the plateau-like feature, seems to be more pronounced for pH ≈ 7.0 and 9.5. Change in slope or formation of plateau-like features is an indication of molecular rearrangements such as molecular tilting or bimolecular layer formation from a compact monolayer at higher π.

Isothermal compressibility, $k = -1/A \times \partial A/\partial \pi$,[53] of the lysozyme monolayers with π variation are calculated from the π–A isotherms for all the three subphase pH conditions and are shown in Fig. 1(b). At very low π value, k sharply decreases and then it maintains nearly a constant value which signifies a transformation of the monolayer from fluid phase (gaseous or LE) to a less compressible LC or solid-like phase. The monolayer at pH ≈ 4.0 seems to be more compressible (corresponding $k =$ 0.022 m mN^{-1}) as compared to monolayers at pH ≈ 7.0 and 9.5 (corresponding $k = 0.017$ m mN^{-1} and 0.016 m mN^{-1}) as obtained at around 15 mN m^{-1}. Upon further barrier compression, another phase transition seems to occur where with an increase in surface pressure compressibility value of the monolayer also goes on increasing but its variation is pH dependent. For pH ≈ 4.0, this phase transition starts to occur after the monolayer experiences a surface pressure of 15 mN m^{-1}, while for pH ≈ 7.0 and 9.5, it occurs comparatively at a higher surface pressure (≈20–23 mN m^{-1}). An increment in compressibility value with an increase in surface pressure primarily indicates the formation of another higher compressible phase and it is pH dependent as can be observed from Fig. 1(b) where the lysozyme monolayer at pH ≈ 9.5 is more compressible than at pH ≈ 7.0 and 4.0. Thus the comparison shows that the nature of the compressibility curves of lysozyme monolayers for three pH conditions is similar as each monolayer transforms from a fluid phase to a less compressible phase and then again to a higher compressible phase upon barrier compression, but not identical.

Reversibility or irreversibility of a monolayer at the air–water interface can be checked from compression–expansion π–A isotherm cycles of the monolayer.[54] Three compression–expansion π–A isotherm cycles of the lysozyme monolayers were examined at $\pi = 33$ mN m^{-1} for three subphase pH conditions (pH ≈ 4.0, 7.0, and 9.5) and are shown in Fig. 2. It is clear from the figure that compression and expansion curves do not overlap and a change in area per molecule is obtained at a specific π value during the expansion of the monolayer resulted in the formation of hysteresis during all three compression–expansion cycles irrespective of subphase pH. With variation in the subphase pH condition, a significant change in the hysteresis area and the lift-off area during 2nd and 3rd compression compared to 1st compression is noticed from the compression–expansion cycles of the lysozyme monolayer. For subphase pH ≈ 4.0, the lift-off area of the monolayer decreases even up to 3rd cycle, however, such decrement in lift-off area with the number of cycles seems to be reduced as the subphase pH approaches the pI of lysozyme, indicating the influence of subphase pH on the hysteresis behaviour of the monolayer.

Understanding on the behaviour of the monolayer and the energy associated with each of the hysteresis cycles can be investigated from different thermodynamic functions involved during the compression and expansion of the monolayer. ΔG_{comp} is basically the energy supplied externally to the system through compressing the monolayer, of which one part ΔG_{expan} is released by the system during expansion after conservation of certain energy in the system, *i.e.*, $\Delta G_{hys} = \Delta G_{expan} - \Delta G_{comp}$. ΔG_{comp}, ΔG_{expan}, and ΔG_{hys} are calculated by taking the surface pressure range from 1 to 33 mN m^{-1} in order to avoid the errors occurring from the fluid portion of the isotherms. Considering the same surface pressure range, the configurational entropy of hysteresis, *i.e.*, $\Delta S_{hys} = \sum_{\pi}[R \ln(A_{exp}/A_{comp})]_{\pi}$ and the enthalpy of hysteresis, *i.e.*, $\Delta H_{hys} = \Delta G_{hys} + T\Delta S_{hys}$ are also calculated.[55] The summary of calculated thermodynamic functions is presented in tabular form in Table 1. It is evident from Table 1 that both ΔG_{hys} and ΔS_{hys} are more negative in the 1st cycle in

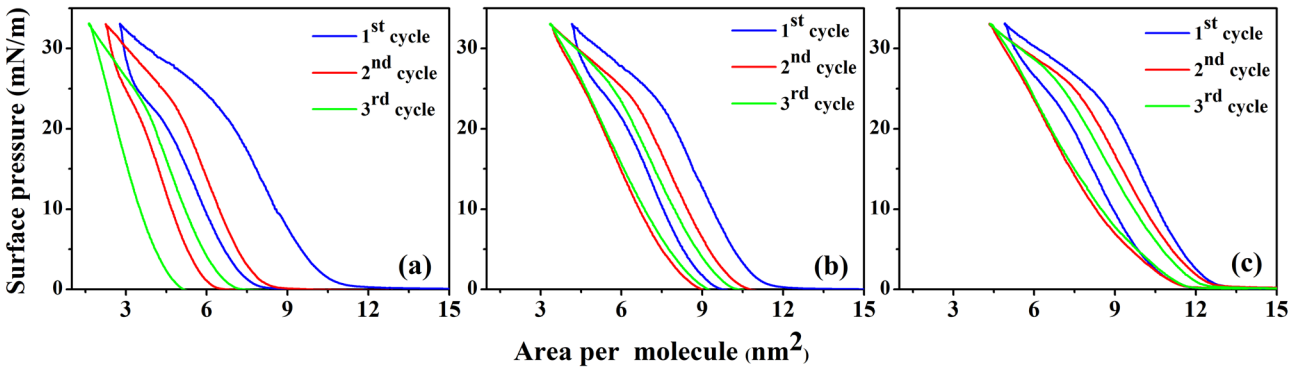

Fig. 2 Compression–expansion π–A isotherms of lysozyme monolayers at pH ≈ (a) 4.0, (b) 7.0, and (c) 9.5 of the subphase. 1st compression–expansion isotherm cycle is indicated by blue color, while 2nd and 3rd compression–expansion cycles are by red and green solid lines respectively.

Table 1 Thermodynamic functions of the lysozyme monolayer calculated from the hysteresis cycle at different subphase pH

Subphase pH	Hysteresis cycle	ΔG_{comp} (kcal mol^{-1})	ΔG_{expan} (kcal mol^{-1})	ΔG_{hys} (kcal mol^{-1})	ΔS_{hys} (kcal mol^{-1})	ΔH_{hys} (kcal mol^{-1})
pH ≈ 4.0	1st cycle	21.434676	10.3907829	−11.0438931	−0.02412	−18.2075331
	2nd cycle	15.47900009	8.42138211	−7.05761883	−0.01962	−12.8847588
	3rd cycle	12.9960311	6.77565933	−6.22037175	−0.02159	−12.6326018
pH ≈ 7.0	1st cycle	19.3055941	11.6063736	−7.69922054	−0.01393	−11.8364305
	2nd cycle	18.8308664	11.6941263	−7.13674011	−0.01445	−11.4283901
	3rd cycle	16.9751125	12.4263578	−4.54875474	−0.009570	−7.39104474
pH ≈ 9.5	1st cycle	21.2908191	14.2073061	−7.08351307	−0.01113	−10.3891231
	2nd cycle	21.4778331	14.2202532	−7.2575799	−0.01228	−10.9047399
	3rd cycle	19.7371648	14.7884879	−4.94867688	−0.008638	−7.51416288

comparison to other cycles. This is probably due to the storage of more amount of energy in the system in order to attain more ordered and compact molecular organization after compression at higher surface pressure, which is also evident from the large hysteresis area from isotherm cycles.

Information on different domain patterns of lysozyme monolayer formed at three subphase pH conditions on the water surface are extracted from BAM images, which are shown in Fig. 3. It can be seen from the 1st column of Fig. 3 that lysozyme molecules at $\pi = 5$ mN m^{-1} during 1st compression form a homogenous monomolecular layer at the air–water interface for all pH conditions. This homogeneity in the monolayer disappears with the increment in surface pressure as the stripe-like patterns start to form at 15 mN m^{-1} for pH ≈ 4.0, while for the other two pH conditions such stripes are formed at $\pi = 20$ mN m^{-1}, as can be seen from 2nd column of Fig. 3. Further increase in surface pressure of the monolayer, the formation of stripe-like patterns continues as a result of which the number of stripe-like patterns or the width of the domain increases with the increment in surface pressure of the monolayer which is quite noticeable from the comparison of 2nd and 3rd column. In addition, with the change in the monolayer texture to stripe-like pattern, intensity variation (*i.e.* appearing bright) in the image is also observed during the compression which indicates the formation of relatively thicker monolayer with increase in surface pressure, which is in accordance with the results reported by Singh *et al.*[38] The stripes formation as well as the thickness increment of the lysozyme Langmuir monolayer with barrier compression is probably due to the occurrence of molecular rearrangement as aggregation, molecular tilting, *etc.* pH dependent comparison study shows that although for pH ≈ 4.0 stripes formation occurs at lower surface pressure than at pH ≈ 7.0 and 9.5 but at higher surface pressure the monolayer at pH ≈ 9.5 possess more number of stripe-like patterns than the other two pH conditions as can be seen from 3rd column of Fig. 3. To visualize the monolayer at $\pi = 5$ mN m^{-1} during 2nd compression, the same monolayer was expanded to the barrier limit followed by compressing it again to that specific surface pressure. With the expansion of the barrier, the number of stripes or width of stripes ceases and the monolayer again appears dark after full expansion. However, less number of stripes still exist over homogeneous pattern even at $\pi = 5$ mN m^{-1} during 2nd compression when subphase pH is ≈4.0. On the contrary, monolayers at pH ≈ 7.0 and 9.5 do not have any trace of stripes, rather homogeneous morphology have been observed at $\pi = 5$ mN m^{-1} during 2nd compression, which is nearly similar to the BAM images of the respective monolayer at the same surface pressure during 1st compression.

To extract the morphological information, films are deposited on silicon substrates at different points of the isotherms for three subphase pH conditions and are characterized by AFM as shown in Fig. 4. Independent of pH, all the deposited films present roughly globular morphology with the globules connecting to each other. Height histogram of each image depicts

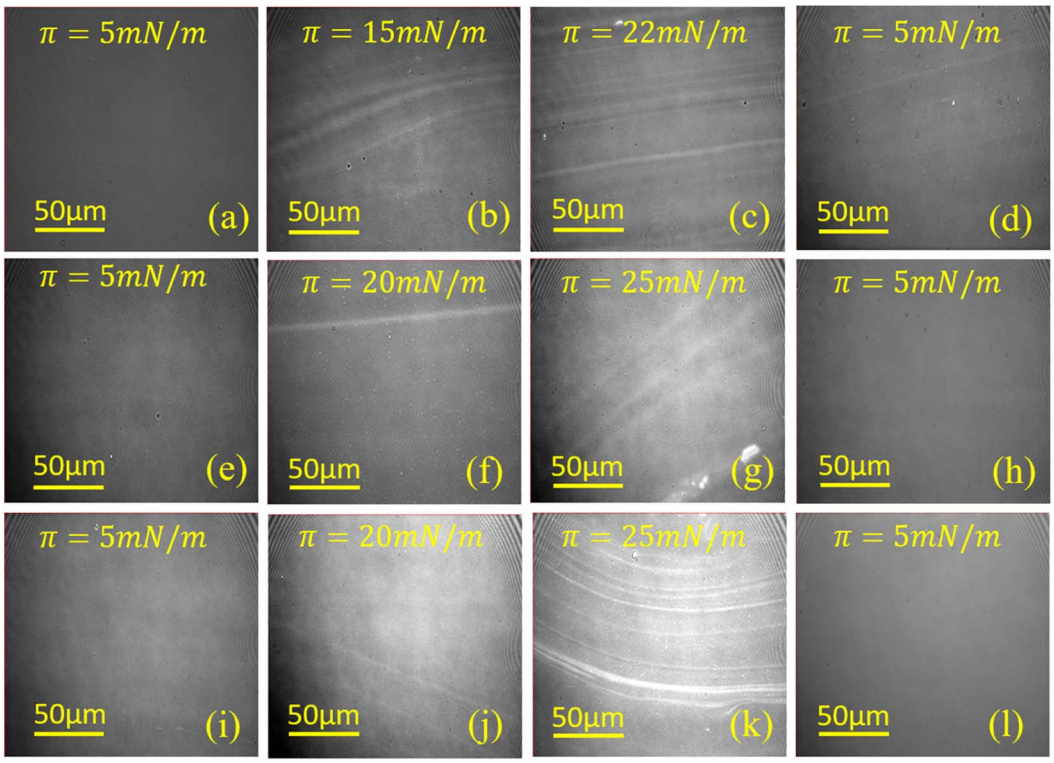

Fig. 3 BAM images of lysozyme monolayers captured at lower, intermediate, and higher surface pressure during 1st compression and again at lower surface pressure during 2nd compression are shown in the 1st, 2nd, 3rd, and 4th column, for three different subphase pH values, *i.e.*, at pH ≈ 4.0 (a)–(d), 7.0 (e)–(h), 9.5 (i)–(l). Bars represent 50 μm.

the average height (h_{av}) of the respective film whereas the *z*-scale bar provides the total height (h_t) information. From Fig. 4(a)–(c) it can be seen that for pH ≈ 4.0, h_{av} of the lysozyme films at lower and higher surface pressures are found to be 0.78 and 0.88 nm with h_t of 1.45 and 2.17 nm during 1st compression, while in 2nd compression deposited at lower pressure h_{av} change to 0.73 nm with h_t of 1.55 nm. For subphase pH ≈ 7.0, h_{av} of 0.78, 1.14 and 0.73 nm are acquired, whereas respective h_t of 1.64, 2.50, and 1.75 nm are found from the protein films deposited at lower and higher surface pressures in 1st compression and also at lower pressure in 2nd compression respectively, provided in Fig. 4(d)–(f). Again, at pH ≈ 9.5, during 1st compression h_{av} of 0.68 and 1.15 nm with h_t of 1.58 and 2.62 nm are obtained at lower and higher surface pressures. However, for the same subphase pH at lower surface pressure during 2nd compression, h_{av} and h_t of 0.78 and 1.61 nm are obtained. Independent of subphase pH, the deposited films always follow the trend that h_{av}, as well as h_t, is always more at higher surface pressure during 1st compression in comparison to lower surface pressure during 1st and 2nd compressions, which may be related to molecular reorganization or tilting. Height information along with r.m.s. roughness (σ) of all deposited protein films are tabulated in Table 2.

Out-of-plane structures of the deposited lysozyme films are obtained from the XRR study shown in Fig. 5. For pH ≈ 4.0, the films deposited at π = 5 mN m^{-1} during 1st and 2nd compressions possess a thickness value of ≈34 Å, while the thickness value increases to 43 Å when deposited at π = 27 mN m^{-1} during 1st compression. For pH ≈ 7.0, the films deposited at π = 5 mN m^{-1} and 27 mN m^{-1} during 1st compression possess a thickness value of ≈36 and 47 Å respectively. However, the thickness value is found to be ≈36.5 Å when the film is deposited in 2nd compression of the same monolayer at π value of 5 mN m^{-1}. The monolayer when deposited at subphase pH ≈ 9.5 over the substrate at π of 5 mN m^{-1} during both 1st and 2nd compression, have a thickness value of ≈35.5 Å, while the thickness of ≈55.5 Å is found for the film deposited at higher surface pressure (π = 27 mN m^{-1}) in 1st compression. Thus, the film thickness after the compression–expansion cycle of the isotherm nearly follows reversible nature but the maximum electron density increases from ≈0.68 to 0.71 e Å^{-3} indicating the increment of the electron density by ≈4.5%, which might be for the elimination of defects during 1st compression of the monolayer. The distribution of EDPs as shown in Fig. 5 signifies that two layers having different electron densities are present, *i.e.*, a lower layer having a higher electron density (≈0.68–0.71 e Å^{-3}) towards solid surface and an upper layer having a relatively lower density (≈0.33–0.46 e Å^{-3}) towards air side. The thickness of the lower layer is around 16–22 Å, while the thickness of the upper layer is obtained as 18–33 Å. The higher density towards the hydrophilic substrate surface is due to the orientation of relatively hydrophilic residues of lysozyme molecule towards the water side and less hydrophilic or hydrophobic residues towards the air side after spreading from the specific three-component solvent.

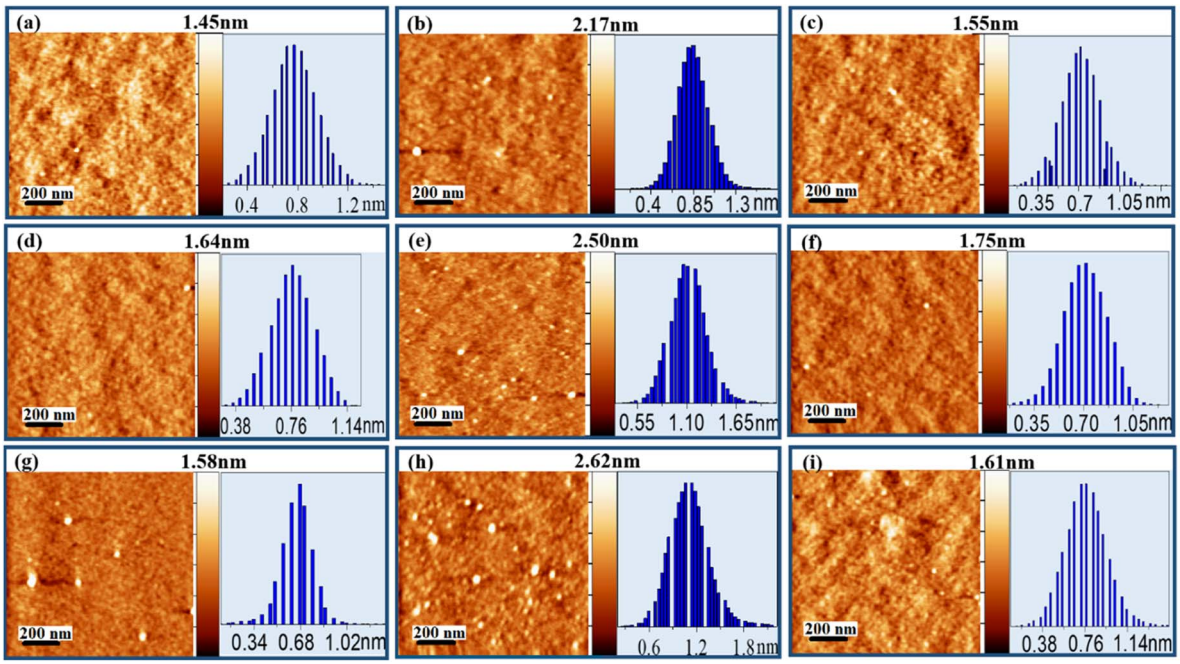

Fig. 4 AFM images of lysozyme LB films deposited on Si (001) at three different pH values, *i.e.*, at pH ≈ 4.0 (a)–(c), 7.0 (d)–(f), and 9.5 (g)–(i). Films deposited during 1st compression at lower and higher surface pressure (*i.e.* at $\pi = 5$ mN m^{-1} and 27 mN m^{-1}) are shown in (a), (d), (g) and (b), (e), (h) respectively, while for the films deposited during 2nd compression of the monolayer at lower surface pressure ($\pi = 5$ mN m^{-1}) are represented in (c), (f), (i). On the right hand of each image, total height or *z*-scale bar as well as height histogram of the respective AFM image are shown. Scan size: 1 μm × 1 μm.

Table 2 Height information and roughness of lysozyme LB films deposited at different subphase pH

Film parameters			r.m.s. roughness, σ (nm)	Average height, h_{av} (nm)	Total height, h_t (nm)
pH	π (mN m^{-1})	Cycle			
≈4.0	5	1st comp	0.14	0.78	1.45
	27		0.15	0.87	2.17
	5	2nd comp	0.14	0.73	1.55
≈7.0	5	1st comp	0.12	0.78	1.64
	27		0.17	1.14	2.50
	5	2nd comp	0.13	0.73	1.75
≈9.5	5	1st comp	0.10	0.68	1.58
	27		0.21	1.15	2.62
	5	2nd comp	0.15	0.78	1.61

Stability of the lysozyme monolayer at the air–water interface is estimated from the normalized specific molecular area–time ($A/A_0 - t$) curves at a constant surface pressure of 27 mN m^{-1} for a period of 1 hour, shown in Fig. 6(a). It is found that a quite stable lysozyme monolayer is formed at the air–water interface having subphase pH ≈ 7.0 as the initial area is reduced by nearly 17% even after the monolayer is allowed to relax for a period of 1 hour. From the *in situ* pattern of the relaxed monolayer at $\pi = 25$ mN m^{-1} which is shown in Fig. 6(b), it is visible that the large number of stripe-like patterns as formed before the monolayer is allowed to relax aggregates with time, resulting in a formation of relatively larger domains. Stability of the lysozyme film after depositing the relaxed monolayer on hydrophilic Si (001) substrates at pH ≈ 7.0 at a constant surface pressure, $\pi = 27$ mN m^{-1} is additionally investigated from the analysis of XRR and AFM shown in Fig. 6(c) and (d) respectively. EDPs shown in Fig. 6(c) show a thickness value of about ≈47 Å for the monolayer deposited after 1 hour which is similar to the thickness value of immediately deposited film. Again Fig. 6(d) shows that the film with the same relaxed condition has an h_{av} of ≈1.2 nm having a h_t of ≈2.74 nm that is comparable to the film deposited immediately at $\pi = 27$ mN m^{-1} shown in Fig. 4(e). Such evidence makes a clear vision regarding the formation of lysozyme film which is stable enough for holding the structure even for a longer time period.

π–*A* isotherms and the corresponding compressibility curves of the lysozyme Langmuir monolayers formed at subphase pH between 4.0 to 9.5 show the transition of the monolayer from

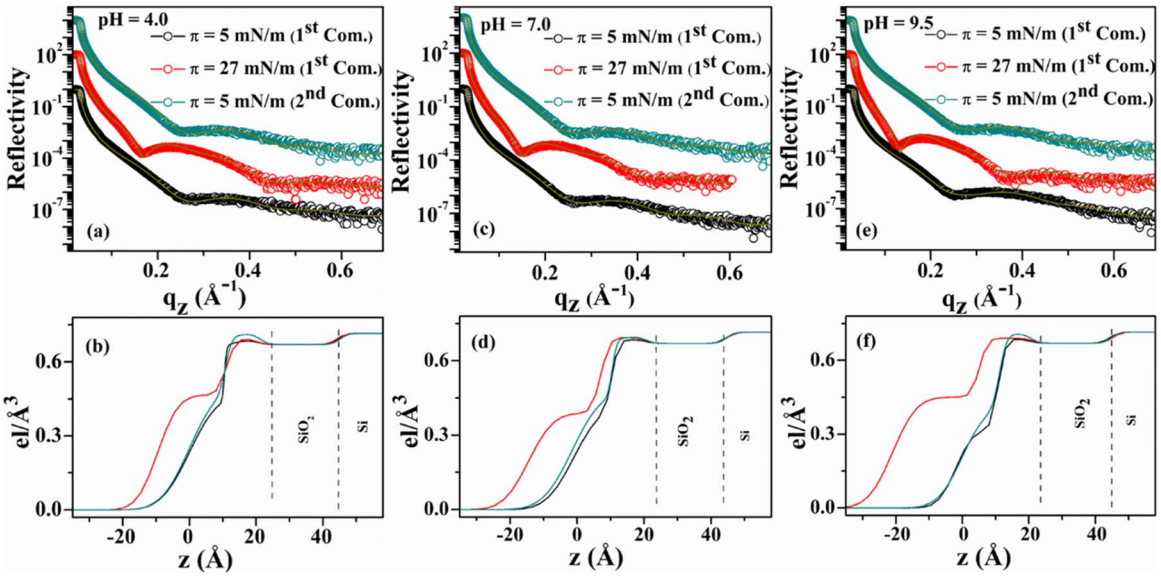

Fig. 5 X-ray reflectivity data (open circles) and the fitted curves (solid lines) of the lysozyme films deposited at three π values, *i.e.*, at 5 mN m^{-1} (black circles) and 27 mN m^{-1} (red circles) during 1st compression and again at π of 5 mN m^{-1} (green circles) during 2nd compression, at subphase (a) pH ≈ 4.0, (c) pH ≈ 7.0 and (e) pH ≈ 9.5. (b), (d) and (f) corresponding electron density profiles (EDPs) obtained from the fitting of the reflectivity data.

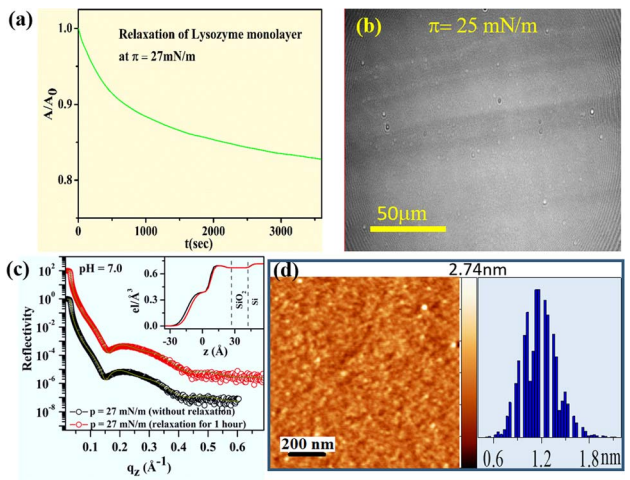

Fig. 6 (a) Stability curve ($A/A_0 - t$) of the lysozyme monolayer formed at the interface of aqueous subphase for 1 hour of time duration at π = 27 mN m^{-1}, (b) *in situ* image of the same monolayer at surface pressure of 25 mN m^{-1} after relaxation for 1 hour as obtained from BAM, (c) XRR data with fitted curves for the film deposited at target pressure of 27 mN m^{-1} without (black circles) and with relaxation (red circles) for 1 hour time period at subphase pH ≈ 7 and respective EDPs are in the inset. (d) AFM image of the lysozyme film fabricated at π = 27 mN m^{-1} after relaxation for 1 hour at the air–water interface and height histogram as well as *z*-scale bar are shown on the right side of the image.

a less compressible phase to a highly compressible phase with increase in π regardless of subphase pH. However, at subphase pH ≈ 4.0, such transition in the monolayer occurs at a relatively lower π value compared to that of pH ≈ 7.0 and 9.5 respectively. Such compressibility variation is actually related to the stiffness/rigidity of the monolayer that depends upon the subphase pH condition as well as on monolayer surface pressure. Compression–expansion isotherm cycles confirm the existence of hysteresis in the lysozyme monolayer formed at different subphase pH conditions, even up to the 3rd compression–expansion π–A isotherm cycle. In addition, a decrease in lift-off area with cycles is perceptible from the isotherm cycles, more prominently visible for the monolayer at pH ≈ 4.0. The nature of the isotherms and irreversible hysteresis behaviour of the monolayers can be correlated to the *in situ* domain pattern of lysozyme monolayer as visible from BAM images. With compression, the loosely packed monolayer turns into a compact monolayer along with the formation of stripe-like domains at higher surface pressures. During expansion, such compactness of the monolayer or the domain patterns tends to hold their structures depending upon the subphase pH conditions, thus producing a decrease in mean molecular area. Different viscoelastic behaviours of monolayers are generally influenced by the presence of domains on the water surface. It was evidenced that the presence of such domains increases the compressibility of the monolayers to a greater extent,[56] which resonance with the results reported in the present study. Compressibility curves shown in Fig. 1(b) show that the monolayer is more compressible at pH ≈ 4.0 around π = 15 mN m^{-1} (*i.e.* before a marked transition) and it can be due to the formation of stripes at 15 mN m^{-1} as visualized in Fig. 3(b), while no such stripes are formed at subphase pH 7.0 and 9.5 even up to π ≈ 18–19 mN m^{-1}, which makes the monolayers comparatively less compressible. However, at higher surface pressure compressible behaviour is more for the monolayer at pH ≈ 9.5 due to the presence of more number of stripes in comparison to the other two pH conditions (pH = 4.0 and 7.0)

as can be seen from Fig. 3(k). Moreover, Fig. 3(d) gives a clear indication of the retention of the stripe-like domains even after compression–expansion–compression of the monolayer, thus, producing a lower lift-off area in each compression–expansion cycle as can be seen from Fig. 2(a). Unlike pH ≈ 4.0, a nearly homogeneous pattern is visible in the monolayer for subphase pH ≈ 7.0 and 9.5 at the same lower surface pressure during 2nd compression. The absence of such domains helps in retaining the initial monolayer configuration as formed during 1st compression–expansion cycle, hence a negligible change in lift-off area can be observed in each of the 2nd and 3rd cycles. In combination with the *in situ* study, *ex situ* characterization of the monolayer using AFM and XRR analysis shows the thickness variation of the deposited lysozyme films on Si (001) substrates with the monolayer surface pressure and subphase pH conditions. Height information as obtained from AFM analysis and EDP shows the deposition of thicker film at higher surface pressure than that of lower surface pressure during 1st and 2nd compression. The increase in film thickness with increased surface pressure is due to the specific molecular orientation of the lysozyme molecules, *i.e.*, specific molecular tilting in the monolayer formed at the air–water interface depending upon the applied pH condition. The amount of such molecular tilting with the increase in π from 5 to 27 mN m^{-1} can be estimated to be from 37° to 87° depending on subphase pH conditions. However, the molecules regain nearly their initial configuration if the π is reduced to its initial lower value and the configuration of the monolayer takes mostly side-on orientation when the monolayer is fully expanded. The maximum thickness of the deposited film is obtained at a higher surface pressure of 27 mN m^{-1} at pH ≈ 9.5, where the molecules take nearly end-on configuration as the thickness becomes ≈55.5 Å. However, at this π value and pH condition, a bimolecular layer may also form where the lower layer is in side-on configuration and the upper layer is in a tilted configuration. All such molecular configurations formed at different surface pressure and subphase pH conditions are schematically shown in Fig. 7. Structural reversibility of the lysozyme film is ascertained by both XRR and AFM as the films deposited at lower surface pressure during 2nd compression have nearly similar thickness value as the films deposited during 1st compression at lower surface pressure.

Here, it is important to mention that different interactions (attractive and repulsive) come into existence which collectively affect the protein monolayer behaviour at the air–water interface. These interactions can arise due to a combination of electrostatic, hydrophobic as well as van-der Waals interaction between molecules depending on the surface pressure and subphase pH conditions. At pH ≈ 4.0, which is far away from the pI of the protein, lysozyme molecules might have been exposed more hydrophobic parts as compared to pH ≈ 7.0 and 9.5 respectively. It is due to this hydrophobic interaction between the molecules which comes into play at lower π values during compression and is responsible for the formation of different stripe-like domains at pH ≈ 4.0. These domains are obtained even at lower π values of π ≈ 15 to 16 mN m^{-1}, which are visible from the BAM images. On the other hand, for pH ≈ 7.0 and 9.5 relatively less hydrophobic interactions may take place at lower π values. Therefore, no such stripe-like domains are obtained around that range of π values for pH ≈ 7.0 and 9.5 respectively, which effectively appears at a π value starting from $\pi = 20$ to 22 mN m^{-1}. With the increase in barrier compression, electrostatic repulsive interaction plays a significant role. At pH ≈ 4.0, the protein molecules acquire net positive surface charge and it is this repulsive interaction that forces the molecules to tilt to a lesser degree with barrier compression. This is well in agreement with the lower thickness of the deposited films from which a maximum tilt of 51° from the EDPs is obtained due to the less tilting of the protein molecules. As pH approaches pI, this electrostatic repulsive interaction becomes inefficient, as the protein molecules acquire less net surface charge. Thus, with compression of the monolayer, the molecules come closer

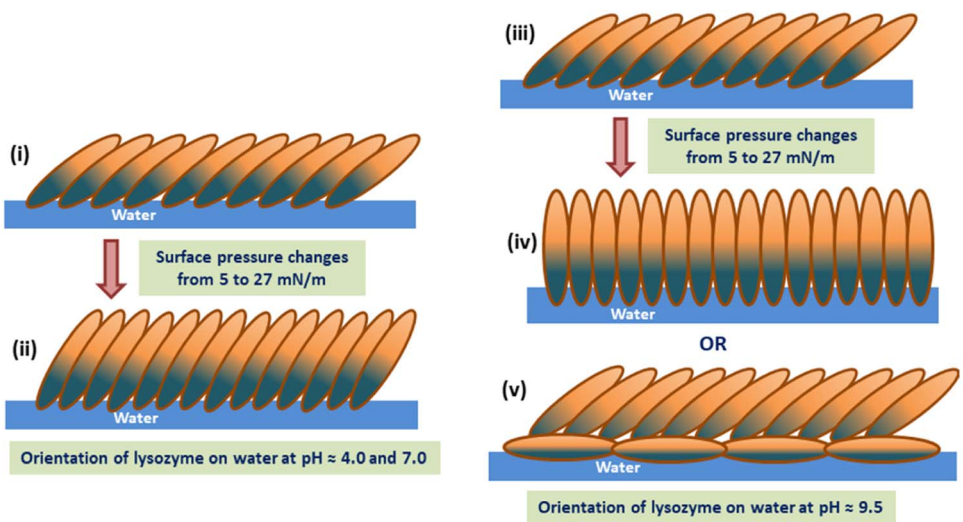

Fig. 7 Schematic representation of the structural modification of lysozyme molecules on water surface under barrier compression at (i) and (ii) subphase pH ≈ 4.0 and 7.0 and (iii)–(v) subphase pH ≈ 9.5.

to each other due to insufficient resistive force, producing a more tilted arrangement of the molecular layer. At a pH value close to the pI of lysozyme, *i.e.*, at pH ≈ 9.5, maximum thickness of the deposited film is obtained, which is estimated to be 87° of tilt at $\pi = 27$ mN m^{-1}, which signifies nearly end-on orientation of the molecules. This molecular tilting at higher surface pressure is associated with the compressibility of the monolayer. From Fig. 1(b) it can be seen that at higher surface pressure the monolayer becomes highly compressible at pH ≈ 7.0 and 9.5. The surface pressure, $\pi \approx 23$ mN m^{-1} marked a transition from a nearly constant compressible film to a highly compressible one for the monolayer at pH ≈ 7.0 and 9.5, while comparatively slow rate of increase in compressibility value beyond $\pi \approx 23$ mN m^{-1} signifies a relatively less compressible film at pH ≈ 4.0. The less influence of electrostatic repulsive interaction at pHs near the pI of the protein upon maximum compression is also responsible for the formation of more number of stripe-like patterns at pH ≈ 9.5 at higher surface pressure, as shown in Fig. 3(k) which is related to the more compressible nature of the monolayer at the macroscopic level for the same condition. However, upon expansion of the monolayer up to a specific barrier position, the hydrophobic, as well as van der Waals interaction, dominates over electrostatic repulsive interaction, which tends to hold the molecular structure towards the lower surface pressure to give rise to different hysteresis areas. The effect of hydrophobic and van der Waals interaction between molecules is found to be more at pH ≈ 4.0, which has been discussed from the point of different domains and large hysteresis area as compared to the other pH conditions. The stability study of the protein shows the capability of the monolayer to remain floating on the water surface for a longer duration of time and also the stable structure of lysozyme monolayer at solid surface as the deposited film after a relaxation time of 1 hour gives nearly similar thickness values, confirmed from AFM as well as XRR analysis. Thus, this study shows the ability of the lysozyme to form a monolayer at the air–water interface from a three-solvent system, which was not possible when dissolved in a polar solvent like water. The study of different structures as obtained from the deposited films will also be helpful in investigating different proteins to be used as protein nano templates, and organic and antimicrobial coating.

4. Conclusions

Globular protein, lysozyme, even after having a small rigid structure can form a stable Langmuir monolayer at the air–water interface from a three-component solvent solution. With the variation of surface pressure and pH condition (pH ≈ 4.0, 7.0, and 9.5), the monolayer behavior has been studied elaborately. A combined force of electrostatics, van der Waals and hydrophobic interactions among the lysozyme molecules play the main role which in turn affects macroscopically the characteristics of the monolayer such as compressibility, hysteresis and stability of the lysozyme monolayer at the air–water interface. A marked phase transition from a lower compressible monolayer to a highly compressible one occurs at a specific surface pressure depending on subphase pH. This phase transition is visualized *in situ via* the transformation of the monolayer from homogenous to stripe-like patterns, as evidenced from the BAM images. Thermodynamic functions evaluated from hysteresis analysis signify that at pH ≈ 4.0 relatively more amount of energy is stored in the system to attain and hold the ordered and compact molecular organization, resulting in more hysteresis amount. In-plane morphology from AFM and out-of-plane structure from XRR of lysozyme film deposited on Si (001) substrate with increased surface pressure confirms the increment in thickness of the film which is relatable to molecular tilting with the increase in surface pressure. Again, the deposition of monolayer during 2nd compression at lower pressure gives nearly similar thickness value as that of the film deposited at the same pressure during 1st compression, confirmed by both AFM and XRR. Such structural reversibility is possible only if lysozyme molecules regain its initial configuration with the expansion of the monolayer. Thus, this study shows the successful fabrication of stable lysozyme monolayers both on water and solid surfaces and also the investigation of its relative structures. This study would be helpful in forming a pure protein nano template in two dimensions and also can be utilized for the purpose of bio coating as lysozyme is a well-known protein having antimicrobial properties.

Author contributions

The author H. Nath has performed all the experiments, analyzed the results, and wrote the manuscript. Author Raktim J. Sarmah has helped in manuscript editing. Dr S. Kundu conceptualized and supervised the work as well as edited and approved the manuscript for communication.

Conflicts of interest

The authors declare that there are no conflicts of interest.

Acknowledgements

H. Nath thanked UGC, New Delhi for the research fellowship and S. Kundu acknowledged the financial support from Department of Science and Technology, Govt. of India. The experimental work is partially supported by Department of Science and Technology (DST), Nano Mission, India (Grant No. SR/NM/NS-1035/2013(G)). The authors would also like to thank IASST, Guwahati for the financial and experimental facilities.

References

1 K. J. Siebert, *J. Agric. Food Chem.*, 2001, **49**, 851.
2 I. Bahar, A. R. Atilgan, R. L. Jernigan and B. Erman, *Proteins*, 1997, **29**, 172.
3 A. V. Guzzo, *Biophys. J.*, 1965, **5**, 809.
4 G. Rabbani, E. Ahmad, M. V. Khan, M. T. Ashraf, R. Bhat and R. H. Khan, *RSC Adv.*, 2015, **5**, 20115.
5 A. S. Yang and B. Honig, *J. Mol. Biol.*, 1993, **231**, 459.
6 M. Weijers, P. A. Barneveld, M. A. Cohen Stuart and R. W. Visschers, *Protein Sci.*, 2003, **12**, 2693.

7 M. van de Weert, J. Hoechstetter, W. E. Hennink and D. J. Crommelin, *J. Controlled Release*, 2000, **68**, 351.
8 A. L. Božič and R. Podgornik, *Biophys. J.*, 2017, **113**, 1454.
9 S. Sarkar and S. Kundu, *JCIS Open*, 2021, **3**, 100016.
10 Y. Desfougeres, A. Saint-Jalmes, A. Salonen, V. Vié, S. Beaufils, S. Pezennec, B. Desbat, V. Lechevalier and F. Nau, *Langmuir*, 2011, **27**, 14947.
11 C. M. Dobson, P. A. Evans and S. E. Radford, *Trends Biochem. Sci.*, 1994, **19**, 31.
12 Y. Chen, Q. Liu, F. Yang, H. Yu, Y. Xie and W. Yao, *Int. J. Biol. Macromol.*, 2022, **200**, 151.
13 Z. X. Lian, Z. S. Ma, J. Wei and H. Liu, *Process Biochem.*, 2012, **47**, 201.
14 W. Huang, S. Ling, C. Li, F. G. Omenetto and D. L. Kaplan, *Chem. Soc. Rev.*, 2018, **47**, 6486.
15 B. K. Paul, D. Ray and N. Guchhait, *Phys. Chem. Chem. Phys.*, 2013, **15**, 1275.
16 M. M. Conde, O. Conde, J. M. Trillo and J. Miñones Jr, *J. Colloid Interface Sci.*, 2011, **361**, 351.
17 R. E. Canfield, *J. Biol. Chem.*, 1963, **238**, 2698.
18 D. C. Phillips, *Sci. Am.*, 1966, **215**, 78.
19 C. C. F. Blake, D. F. Koenig, G. A. Mair, A. C. T. North, D. C. Phillips and V. R. Sarma, *Nature*, 1965, **206**, 757.
20 C. Redfield and C. M. Dobson, *Biochemistry*, 1990, **29**, 7201–7214.
21 M. B. Pepys, P. N. Hawkins, D. R. Booth, D. M. Vigushin, G. A. Tennent, A. K. Soutar, N. Totty, O. Nguyen, C. C. F. Blake, C. J. Terry, T. G. Feest, A. M. Zalin and J. J. Hsuan, *Nature*, 1993, **362**, 553.
22 N. B. Omali, L. N. Subbaraman, C. Coles-Brennan, Z. Fadli and L. W. Jones, *Optometry and Vision Science*, 2015, **92**, 750.
23 E. N. S. Abeyrathne, H. Y. Lee and D. U. Ahn, *Poult. Sci.*, 2013, **92**, 3292.
24 C. A. Haynes and W. Norde, *Colloids Surf., B*, 1994, **2**, 517.
25 R. L. Kayushina, Y. Khurgin, G. Sukhorukov and T. Dubrovsky, *Phys. B*, 1994, **198**, 131.
26 E. E. Uzgiris and R. D. Kornberg, *Nature*, 1983, **301**, 125.
27 A. Tronin, T. Dubrovsky, C. De Nitti, A. Gussoni, V. Erokhin and C. Nicolini, *Thin Solid Films*, 1994, **238**, 127.
28 R. J. Sarmah and S. Kundu, *Food Hydrocolloids*, 2022, **131**, 107788.
29 K. Ariga, Y. Lvov and G. Decher, *Phys. Chem. Chem. Phys.*, 2022, **24**, 4097.
30 K. Ariga, J. P. Hill, M. V. Lee, A. Vinu, R. Charvet and S. Acharya, *Sci. Technol. Adv. Mater.*, 2008, **9**, 014109.
31 A. Ulman, *Chem. Rev.*, 1996, **96**, 1533.
32 C. Nicolini and E. Pechkova, *J. Nanosci. Nanotechnol.*, 2006, **6**, 2209.
33 E. Pechkova, P. Innocenzi, L. Malfatti, T. Kidchob, L. Gaspa and C. Nicolini, *Langmuir*, 2007, **23**, 1147.
34 J. R. Lu, T. J. Su, R. K. Thomas, J. Penfold and J. Webster, *J. Chem. Soc., Faraday Trans.*, 1998, **94**, 3279.
35 S. A. Holt, M. J. Henderson and J. W. White, *Aust. J. Chem.*, 2002, **55**, 449.
36 J. R. Lu, T. J. Su and B. J. Howlin, *J. Phys. Chem. B*, 1999, **103**, 5903.
37 M. D. Lad, F. Birembaut, J. M. Matthew, R. A. Frazier and R. J. Green, *Phys. Chem. Chem. Phys.*, 2006, **8**, 2179.
38 A. Singh and O. Konovalov, *Soft Matter*, 2013, **9**, 2845.
39 T. Yamashita and H. B. Bull, *J. Colloid Interface Sci.*, 1967, **24**, 310.
40 G. Thakur, C. Wang and R. M. Leblanc, *Langmuir*, 2008, **24**, 4888.
41 A. S. Boikova, Y. A. D'yakova, K. B. Il'ina, M. A. Marchenkova, A. Y. Seregin, P. A. Prosekov, Y. A. Volkovsky, Y. V. Pisarevsky and M. V. Koval'chuk, *Crystallogr. Rep.*, 2018, **63**, 719.
42 E. Pechkovaa and C. Nicolini, *J. Cryst. Growth*, 2001, **231**, 599.
43 G. D. Fidelio, B. Maggio and F. A. Cumar, *Chem. Phys. Lipids*, 1984, **35**, 231.
44 K. Das and S. Kundu, *Colloids Surf., A*, 2016, **492**, 54.
45 I. Horcas, R. Fernández, J. M. Gomez-Rodriguez, J. W. S. X. Colchero, J. W. S. X. M. Gómez-Herrero and A. M. Baro, *Rev. Sci. Instrum.*, 2007, **78**, 013705.
46 L. G. Parratt, *Phys. Rev.*, 1954, **95**, 359.
47 J. Daillant and A. Gibaud, *X-ray and neutron reflectivity principles and applications*, Springer, Berlin, New York, 1999, vol. XXIII (331 p.), p. 1.
48 M. Tolan, *X-ray scattering from soft-matter thin films*, Springer, Berlin, 1999, vol. 148, p. 5.
49 J. K. Basu and M. K. Sanyal, *Phys. Rep.*, 2002, **363**, 1.
50 S. Kundu, A. Datta, M. K. Sanyal, J. Daillant, D. Luzet, C. Blot and B. Struth, *Phys. Rev. E: Stat., Nonlinear, Soft Matter Phys.*, 2006, **73**, 061602.
51 S. Kundu, A. Datta and S. Hazra, *Langmuir*, 2005, **21**, 5894.
52 S. Pandit, S. Kundu, S. Abbas, V. K. Aswal and J. Kohlbrecher, *Chem. Phys. Lett.*, 2018, **711**, 8.
53 T. H. Chou and C. H. Chang, *Colloids Surf., B*, 2000, **17**, 71.
54 H. J. Galla, N. Bourdos, A. Von Nahmen, M. Amrein and M. Sieber, *Thin Solid Films*, 1998, **327**, 632.
55 E. J. Grasso, R. G. Oliveira and B. Maggio, *Colloids Surf., B*, 2014, **115**, 219.
56 A. S. Luviano, J. Campos-Terán, D. Langevin, R. Castillo and G. Espinosa, *Langmuir*, 2019, **35**, 16734.